14. EXPERIMENTAL PHYSICS AND TECHNOLOGICAL DEVELOPMENTS ON ULTRA INTENSE LASERS, RADIATION SOURCES, PLASMA BASED ACCELERATORS AND BIOMEDICAL OPTICS

J. T. Mendonça (Head), J. M. Dias, M. Fajardo, G. Figueira, N. Lopes, R. A. Fonseca, J. A. Rodrigues, L. O. Silva, L. Cardoso, J. Wemans, C. Leitão, N. Lemos, F. Wahaia, E. Abreu, N. Brites, R. Macedo, J. Sampaio, A. Smith, F. Viola

14.1. INTRODUCTION

Research in experimental physics at GoLP/CFP covers fundamental and applied aspects of lasers, laser-plasma interactions, intense x-ray and vuv sources, biomedical optics, as well as technology developments for the support of these activities. A significant part of this work is associated with the activities of the Laboratory for Intense Lasers (L2I), the central experimental infrastructure maintained by GoLP. The key aspects of research in 2005 dealt with:

- Laser physics and laser technology;
- X-ray and VUV sources and their interaction with plasmas;
- Plasma channels for laser-plasma accelerators;
- Tunable radiation sources;
- Biomedical optics

14.2. LASER PHYSICS AND LASER TECHNOLOGY

14.2.1 Mirrorless tilted-pulse-front single-shot autocorrelator

Ultrashort pulses exhibiting angular dispersion have their pulse front tilted relative to the phase front. This leads to a serious degradation in the focused peak power, making the use of adequate diagnostics indispensable.

We have developed an upgrade to a previously demonstrated autocorrelator for ultrashort laser pulse-width measurements that extends its versatility, by making it suitable for detecting and correcting tilted pulse fronts. The device, called *a tilted-pulse-front single-shot autocorrelator* (TPF-SSAC) can be used to detect tilts in pulse fronts and perform pulse autocorrelation along any arbitrary direction.

The principle of the TPF-SSAC is to decouple the measurements of the autocorrelation shape and the amount of pulse-front tilt: One of the replicas is flipped in both planes, and the tilt is detected in each direction at a time by correlating the replicas in the orthogonal direction. In this fashion, the presence of a tilt will result in an oblique autocorrelation, as shown in the figure below.

Our modification consisted in introducing two orthogonal Dove prisms to provide horizontal and vertical flipping, converting this autocorrelator into a TPF-SSAC. The figure 14.1 shows this experimental arrangement.

We have used this modified TPF-SSAC to optimize the alignment of the grating compressor of our terawatt CPA laser. We found that initially there was a small pulse-front tilt present in our compressed pulse, which was easy to correct with the aid of this diagnostic. The resulting autocorrelation trace is shown in Figure 14.1.

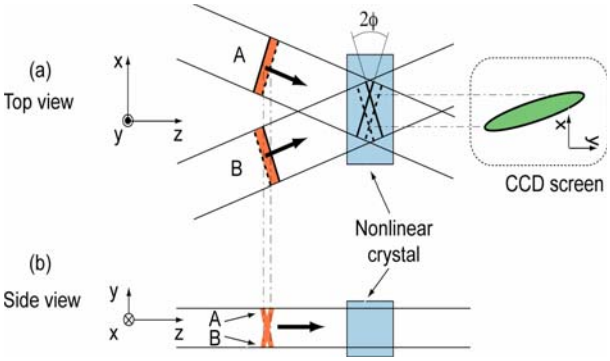

Figure 14.1 – Schematic of tilted pulse front autocorrelator geometry.

To illustrate the capability of the device, we have also acquired a trace of the autocorrelation for a large front tilt, introduced by deliberately deviating the grating pair from parallelism and correcting for the resulting change in their separation in order to obtain the shortest autocorrelation, also shown in the Figure 14.2. From this, we can appreciate that the actual trace width does not change significantly from the corrected version, which illustrates the necessity of using this kind of autocorrelator.

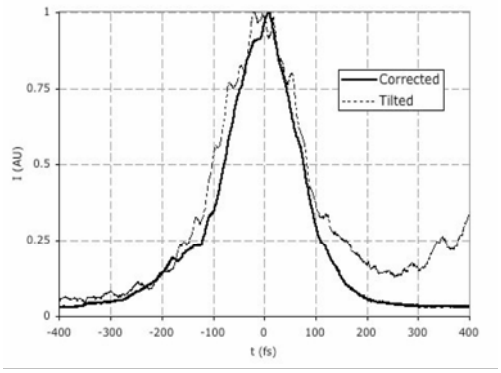

Figure 14.2 - Autocorrelation traces of corrected (solid line) and tilted (dashed line) pulse fronts

14.2.2 OPCPA at GoLP

Optical parametric processes are not new, but their application in laser amplification, especially in high power pulses, is quite recent. Optical parametric amplification can combine a very high gain per pass, tunability and a

broad bandwidth. Adding to it the chirped pulse amplification technique to avoid the inconvenience of excessive peak power inside the laser system, and we have a versatile and relatively efficient way to achieve short, high power laser pulses. Due to the short path needed inside the amplifying media (Figure 14.3), femtosecond pulses suffer little distortions and lengthening, enabling petawatt range pulses to be raised out of the energy of mere terawatt range pump beams.

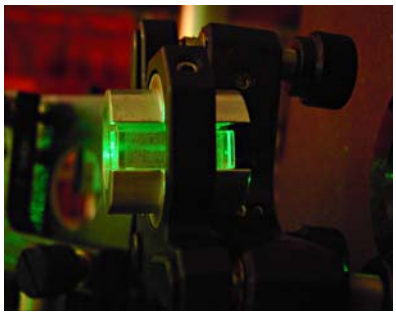

Figure 14.3 - BBO non-linear crystal: the amplifying media where the green pump beam transfers its energy to the infrared signal beam.

Presently we want to demonstrate we can master this promising technique by running mid power amplifiers and comparing the experimental against the expected theoretical results. The equipment in the current setup is likely to become part of some future secondary/probe beam, provided a new pump beam is made available.

Concurrently, there are plans to use OPCPA as an "upgrade" to L2I's multi terawatt laser system, whose beam, the whole or in part, would be used as a pump for a possible petawatt range system.

14.2.3 Ultra Broadband OPCPA – from the theory to the demonstration

The creation of a 3D compatible simulation code for the better understanding of the OPA process provided the conditions to find a new geometry allowing the amplification of ultra broadband pulses. Usually both signal and pump are input in the crystal propagating at given fixed directions which, in general, allows a quite limited gain bandwidth. But the optimum input angle actually varies rather smoothly and predictably with the signal wavelength. It is then possible to angularly disperse the broadband signal, with a grating for example, to interact with the pump beam at close to the optimum angle over a large bandwidth.

To demonstrate this concept we use a slightly modified version of our first OPCPA setup, but we also need to get a broadband signal. That is being arranged by a photonic crystal fibre tailored to generate white light supercontinuum out of our sub-20 nm wide, ~100 fs oscillator.

This technique will enable the simultaneous amplification of wavelengths spanning for almost one octave (Figure 14.4). This will allow *the construction of tuneless amplifiers for tunable narrow band oscillators* or, exploring its full potential, the support of sub-10 fs pulses with excellent contrast.

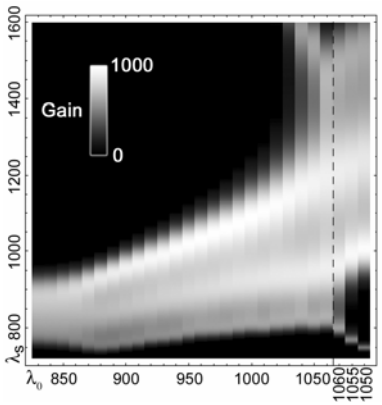

Figure 14.4 - Spectral gain profile (λS/nm) vs. reference signal wavelength (λ0/nm), when signal angular dispersion is optimised for the broadest bandwidth in BBO pumped with 532 nm.

14.2.4 Characterization of the dynamical behavior of diode pumping induced thermal lens on a Yb:phosphate glass[1]

We measured *the characteristic focal length of the thermal lens effect induced in a Yb:phosphate glass pumped by a high intensity diode laser pulse* (Figure 14.5). Because the glass is the active material of a laser amplifier setup its was necessary to define some special characteristics of the thermal effect: the ideal amplification section in the glass where the thermal lens effect is constant; the temporal dynamics of the effect during a single pump pulse and through the first warm-up pump cycles; the dependence of the effect with the pump intensity. The overall goal of the study was to provide vital information about the thermal effects that can be applied in improving the performance of laser amplifiers based on this active medium and pump setup.

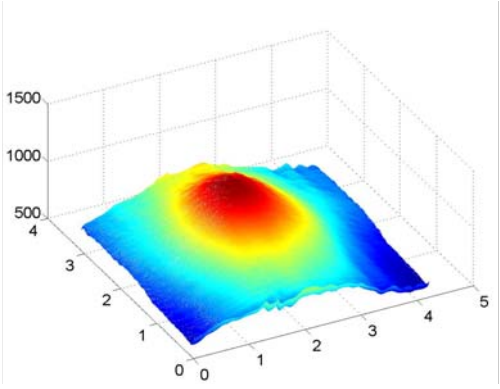

Figure 14.5 - 3D visualization of the wavefront distortion induce to the laser beam during one pass trough the glass at full pump.

[1] Work carried out collaboration with the Polaris group in the Institut für Optik und Quantenelektronik, Jena

The treatment of the interferometric data showed the presence of induce thermal lens with focal distances of 1.5 m at full pump power and uniform in a 1.5 mm diameter section of the glass. The temporal behaviour of the thermal lens was measured and the dependence with the pump intensity defined.

14.2.5 Dual Nd:glass rod amplifier operation of L2I's laser chain

The electronics and software at L2I was initially designed and assembled for firing a single Ø16 mm Nd:glass laser amplifier from Quantel, based on a synchronous handshake pattern between a main computer with Labview® software and the digital delay generator controlling the sequencing of the laser pre-amplifier. The signals were received and processed at L2I's main electronic console, and the firing event – involving charging the capacitor banks, receiving an end-of-charge confirmation, and providing a synchronous firing order – was transmitted via fibre optics to receiver boxes located inside the amplifier power units.
The addition of a new Ø45 mm amplifier, also from Quantel, required a *modification in the triggering electronics:* although coming from the same manufacturer, the two amplifiers were based on technologies that were a few years apart. The electronic upgrade was performed at the level of the amplifiers' receiver boxes, in order to trigger simultaneously both amplifiers and preserve the original handshake pattern. The use of two of these receiver boxes was found to cause electronic offset levels in the triggering signals; in order to solve this, new optical-to-electrical conversion circuits were designed and built, which produce a single control signal.

14.2.6 Setup, alignment and characterization of a high power CW Nd:YLF laser

In March 2005 we received two high power Neodymium:YLF laser oscillators donated by the Central Laser Facility (CLF) of the Rutherford Appleton Laboratory. Their high power (>10 Watts, continuous) allows the beam diameter to be expanded to several centimetres, which is ideal for aligning the high-energy stages of the L2I laser. In particular, the diffraction gratings used in the compressor must be aligned with a precise reference wavelength.

These high power lasers demanded considerable requirements in terms of three-phase power consumption and water cooling, which together with the physical size of their power supplies led to a remodelling of the laboratory room where they are housed.

The lasers required a number of replacement components and a detailed evaluation of their operating procedure.

The laser was further characterized in terms of the efficiency (Figure 14.6) and beam shape of the various modes. For the TEM00 mode, an evaluation of the role of the Fresnel number of the cavity in the efficiency was also performed, by adjusting an intra-cavity aperture. The measurement of the beam shapes for the several cases allowed us to determine the effective beam intensity.

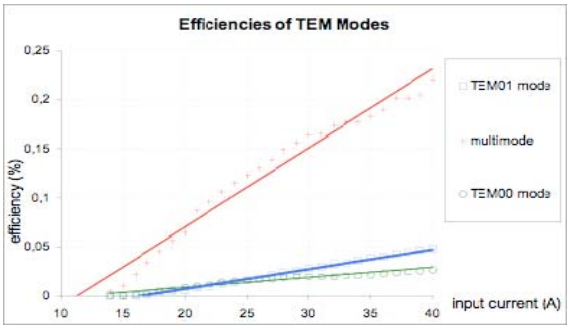

Figure 13.6 - Efficiency of the several lasing modes as a function of the input current.

14.3. X-RAY AND VUV SOURCES AND THEIR INTERACTION WITH PLASMAS

14.3.1 Novel XUV Sources: Second Generation X-ray Lasers

High Harmonic Amplification is shown in an Optical-Field Ionized X-ray laser. The 4d-4p X-ray line of Kr at 32.8 nm, which has a close match to the 25th harmonic of the infrared laser, was amplified up to 200 times. Energy extraction regime was also achieved, depending on the level of seeding. This *second-generation X-ray laser* is fully polarized, has low divergence and shows a high degree of coherence. The duration is also expected to be short, fulfilling the requirements for *an ultra-intense tabletop X-ray laser.* Conditions for higher energetic output are also suggested.

In the experiment shown (Figure 14.7), we have used, for this second generation X-ray laser, a well-characterized, short-pulse, coherent and polarized High Harmonic seed, an image relay to focus the harmonic pulse onto the amplifier plasma, and a low-density amplifier medium with a population inversion in the XUV, which keeps the perfect optical properties of the seed.

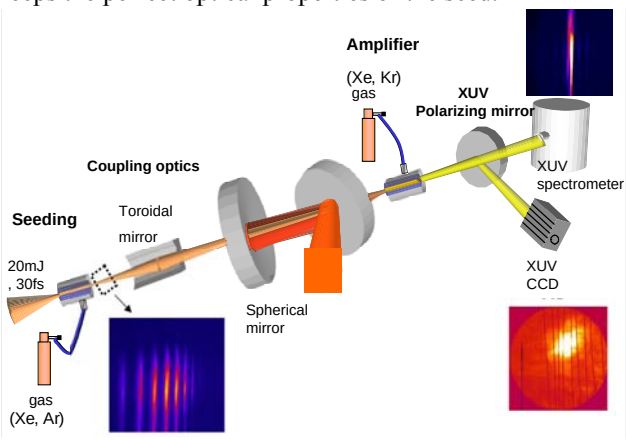

Figure 14.7 - Experimental setup for seeded optical field. ionization x-ray laser at Laboratoire d'Optique Appliquée

We have shown that tabletop X-ray lasers have reached a second generation by extending the concept of an optical laser chain to the XUV. The seeded X-ray laser is a new X-ray source, which may serve as a lower intensity complement to the forthcoming XUV-FELs. While further studies must be made to determine the amplified pulse duration, due to the high optical properties of the beam we may expect to reach unprecedented XUV intensities on a tabletop, allowing to bridge the gap between current X-ray sources and future ultra-bright XUV free electron lasers.

14.3.2 X-ray Optics: VUV FEL wavefront measurements

We have characterized for the first time the wavefront of an XUV Free Electon laser (Figure 14.8). The experiment was performed at DESY in November 2005.

A 30 nm VUV Free Electron Laser was focused using a grazing incidence toroidal mirror. The resulting divergent beam was propagated under vacuum onto a Hartmann plate followed by a back-thinned, cooled CCD. The full beam coming from the XUV toroidal mirror was then recorded. Several shots were made showing a beam fluctuation over 200mrad, incompatible with usage of the beam for high intensity focusing. As saturation of the laser was not achieved during the course of the experiment, a better performance is expected for future experiments.

The VUV-FEL mean energy was around 5μJ. Using a noble gas in the beam path as attenuator, we were able to record *single-shot measurements of the VUV FEL wavefront* for the first time.

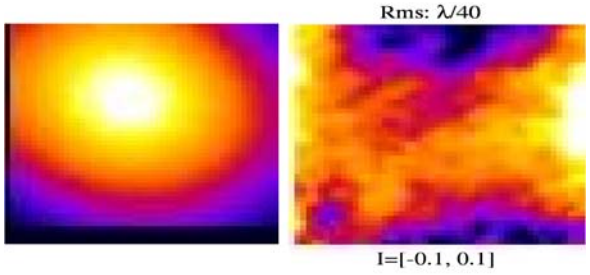

Figure 14.8 - Raw data for wavefront measurement using spherical wavefront (sensor calibration). Left: intensity on sensor; right: wavefront displacement in units of λ

14.4. PLASMA CHANNELS FOR LASER-PLASMA ACCELERATORS

14.4.1 Capillary plasma discharges for electron accelerators[2]

The development of compact laser-plasma electron accelerators in the GeV range is an important step in the accelerator research after the recent demonstration of the capability of these accelerators to produce monochromatic electron bunches in recent experiments. These energies can be obtained by extending the acceleration length well beyond of the Rayleigh length, using some type of guiding.

A new set of *guiding devices for ultra intense lasers* was designed, built and tested (Figure 14.9). These devices use a set of glass capillaries (aligned to a common axis) about 2.5 mm long separated by 0.8 mm gaps and located between two conic-shaped metallic electrodes with a hole on the apex. The distance between the electrodes and the first and last capillary surfaces is 0.2 mm. The plasma in the gaps between the capillaries can be imaged to outside and probed by a laser beam orthogonal to the device axis (Figure 14.10).

These guiding devices need an extensive dynamic characterization using different high-voltage pulses, hydrogen pressures and filling times. However, this preliminary results show guiding for distances up to 1 cm at plasma densities compatible with GeV energy gains. The use of these devices for high-intensity laser propagation are the objectives of 2006 research.

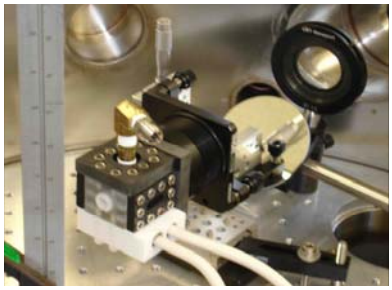

Figure 14.9 - Picture of a 1 cm plasma channel prototype mounted in the target chamber

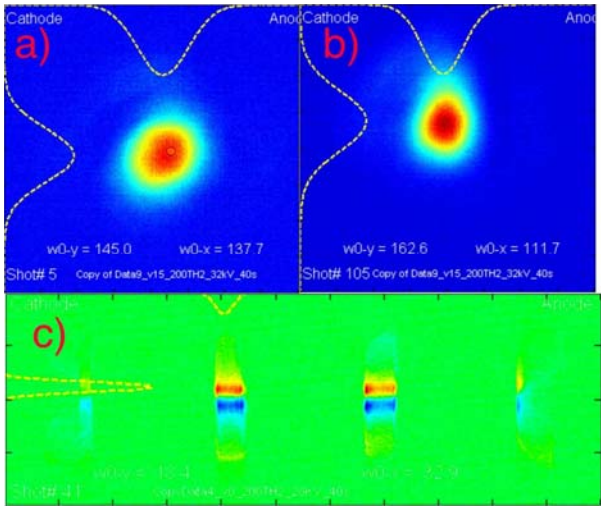

Figure 14.10 - a) image of f/50 focal spot taken at capillary entrance; b) image of laser beam taken at exit of capillary showing light focusing due to interaction with plasma; c) Schlieren image of plasma capillary obtained by propagating a probe beam through the capillary gaps perpendicularly to the plasma channel axis.

[2] Work performed in collaboration with F. Fang, and C. Clayton (UCLA).

14.4.2 Development of a short pulse high-voltage source for plasma channels[3]

The goal of the project described here is the development of a device to generate *ultra-short high-voltage (HV) pulses to produce plasma channels.* A functional discharge-based plasma channel requires a high-voltage pulse in excess of 30 KV/cm with steep rising and low jitter. Our goal is to develop the channel in two stages: first, a high voltage (50KV), high impedance (400Ω) and short (10ns) pulse will ionize the plasma and secondly, a high current (≥200A) capacitive discharge will heat the plasma during up to 150 ns, creating a suitable plasma density profile for guiding high intensity laser light.

The system is composed of 4 main parts: an HV source (off-the-shelf), a pulse forming switch, which has to be fast and low in resistance, a transmission-line transformer (TLT), which increases the amplitude of the pulse to the final voltage and a shockline which shapes the pulse, shortening its risetime (Figure 14.11).

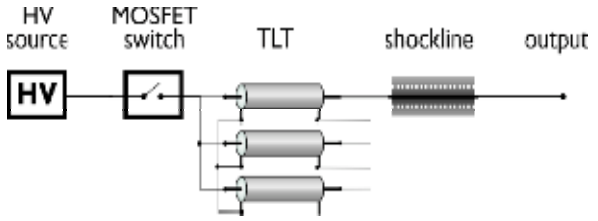

Figure 14.11 - General arrangement of the several components of the device

Although several HV switch technologies can be used, the use of MOSFET technology is considered the most promising for our parameters. In comparison to the thyratron technology it presents shorter risetime, lower jitter and allows to control the opening of the switch and therefore the discharge duration.

Figure 14.12 - MOSFET switch module, showing 7 MOSFET units. The main MOSFET is seen on top, and part of the protection and driving circuitry is directly below

The first prototype devices were built at UCLA. They were used to study the behavior and operational limitations of the several components and to test the device as a whole.

Two switch prototypes were built. The first, conceived only to test the feasibility of the design, consisted of only 4 MOSFET switches in series and its respective triggering and protection system. The second switch was composed by 14 MOSFETs in series, capable of a stand-off voltage of 10KV (Figure 14.12).

A HV ultrashort electric pulse generator was conceived and a first prototype was built. This has allowed for the demonstration of this technology as possibility for current experiments on the generation of plasma channels.

14.5. TUNABLE RADIATION SOURCES

14.5.1 Relativistic Mirror for THz Radiation Sources[4]

The Strathclyde Terahertz to Optical Pulse Source (TOPS) at the Scottish University of Strathclyde in Glasgow, is one of the few facilities in Europe that provides high power few-cycle visible and near-infrared laser sources, together with sub-cycle electromagnetic pulses in the far infrared (mm-wave or terahertz spectral region). We have started this collaboration in order to perform experiments on the production of *relativistic mirrors generated by ionization fronts, for sub-cycle terahertz radiation pulses.* The aim of those experiments is to obtain sub-cycle visible radiation by the double Doppler relativistic effect.

During this year we have installed the experimental setup for generating the ionization fronts (Figure 14.13). The ionization fronts were produced in a pulsed supersonic gas jet (Mach 3) of Argon inside a vacuum chamber. In order to characterize the generated plasma a Mach-Zehnder interferometer was installed in the diagnostic beam. The spectral contents of the ionization pulse were also recorded using a spectrometer. Several plasma profiles and spectra were obtained. In parallel we have started preliminary simulations in the EPP cluster using the Osiris 2.0 code reproducing the experimental conditions.

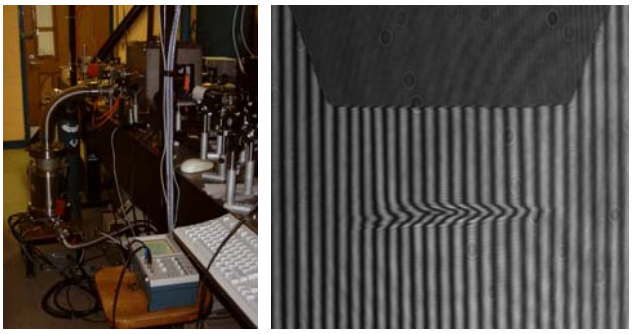

Figure 14.13 - Experimental setup (left) and interferogram of the plasma in the gas jet (right)

14.5.2 Design and characterization of gas jets for laser-plasma interactions

Experiments on high intensity laser-gas interaction require the use of sharp edge and well-defined pulsed gas jets in order to avoid ionization induced refraction and achieve the maximum intensity on the focal spot. *Supersonic Laval nozzles* can produce sharp gas jets in vacuum with uniform gas density and are suitable for many applications.

[3] Work carried out in collaboration with C. Clayton (UCLA)

[4] Work performed in collaboration with D. Jarozinsky's group (U. Strathclyde)

To analyse the interferograms obtained from the Mach-Zehnder interferometer it was developed an automatic fringe-pattern analysis code.

Observing the density profiles for different initial pressures applied to the nozzles, it was possible to see three different nozzle flows (overexpanded, ideal, underexpanded). As predicted by the theory, the ideal and the underexpanded flows were the ones that had less shock waves.

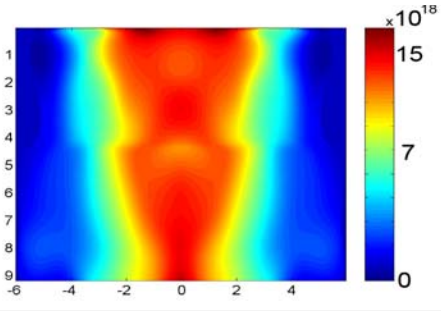

Figure 14.14 - Density profile of a Laval nozzle (8mm exit diameter)

14.6. BIOMEDICAL OPTICS

14.6.1 Axial myopia reduces laser dose in the photodynamic therapy[5]

Pathologic myopia is diagnosed when axial length of the eye is greater than 26,5 mm and when distance acuity is greater then 6 diopters. This rare type of myopia, in which the eyeball continues to elongate, has been reported to be a major cause of blindness in young patients. Nowadays the most popular treatment to CNV is photodynamic therapy (PDT). The PDT therapeutic standard protocol consists in administrating Visudyne® by intravenous injection, followed by application of a non-thermal red laser light (λ=689 nm) with an irradiance of 600 mW/cm2 (Figure 14.15).

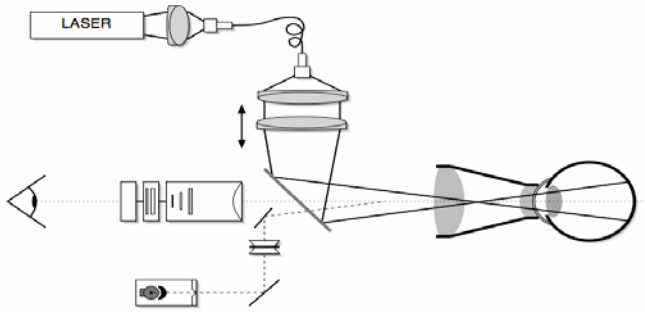

Figure 14.15 - Schematic diagram representing the output laser system, the slit lamp, the accessory Mainster lens and the patient's eye in the PDT treatment.

As the refractive eye's power is one of the main factors that determine the size of laser spot in the retina and its irradiance power, it should be taken in consideration, especially in pathologic myopic eyes. Moreover the eyes that had been corrected with intraocular lens implants, had also suffered significantly changes in their refractive power. One important question that arises is how these changes can affect the laser spot size and irradiance in the PDT treatment. In this work we evaluate not only the *influence of eye's axial length in laser spot size in retina and variation in laser irradiance in PDT in high myopia, but also to study the influence of intraocular lenses in induction of laser dose reduction in this treatment.*

For the optical model we have used Liou and Brennan model, among other corrections to match our problem. These models were integrated using Oslo-LT Edition 6.1 optical design software (Lambda Research Corporation).
The increase of eye's axial length implies an increase in laser spot size in retina with a linear correlation. Consequently, for the same output laser power, the irradiance changes inversely with the square of the projection size of the laser spot in the retina. For operated eyes with the corrective pseudophakic implantation will increases even more the retinal laser spot dimension, and consequently will aggravate the induced irradiation reduction.

This study demonstrate that axial length of the eye reduces progressively the light dose in photodynamic therapy. The axial length is an important factor to take in consideration for ensuring, safety, reproducibility of clinical results and optimization of photodynamic therapy in high myopics eyes. Therefore the axial length is an important parameter that should be taken in to account for the elaboration of future Visudyne treatment protocols in pathologic myopia.

14.6.2 Diffraction enhanced imaging

Point-source X-ray radiography is a well established technique for probing dense objects, and laser-produced Kα sources, with time resolution down to 2 ps, have been used for X-ray imaging of biological objects [1] or dense plasmas [2]. The incident radiation is partially absorbed by the object, and the transmitted image depends on the object's thickness and constitution. However, these images lack definition, namely at the borders of the object, due to poor contrast of X-ray absorption far from absorption edges.

Our aim is to achieve the same *enhancement in contrast* on the object's structure, *by means of a Bragg crystal.* A numerical analysis of the imaging experience was made, using a 7 Å x-ray plasma as light source, and a TLAP crystal (d = 25.8 Å) for the phase shift enhancement. Two objects were considered: a simple cylinder (made of SiO2, with a 5μm radius) and an empty cylinder (made of SiO2, with a 5μm outside radius and a 2μm inside radius). For these two objects it was possible to compare absorption and phase contrast images (Figure 14.16).

The results obtained for the simple cylinder were equivalent to the ones shown above with a capillary. The

[5] Work carried out in collaboration with António Castanheira Dinis (CECV-FML), João Nascimento (Instituto Gama Pinto), Pedro Reis (ALM)

enhanced phase contrast technique clearly represents a gain in definition for the borders and the details inside the object. Moreover, these results correspond to 78 photon/pixel or 97 photon/pixel maximum photon densities on the detector, for the simple and empty cylinder respectively, meaning this experience could be made with a single shot.

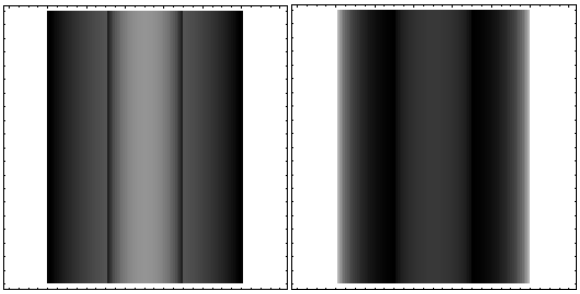

Figure 14.16 - Image of an empty cylinder: left) with absorption alone; right) with absorption and enhanced phase contrast

14.6.3 Optical aberrations: wavefront reconstruction and simulation of visual acuity[6]

All optical systems suffer from aberrations that limit the quality of the image produced. The human eye, besides its complex and exquisitely designed optical system, is no exception. Surprisingly, our visual system has a poor image quality by comparison to man-made optical systems. Visual acuity is defined as the spatial resolving capacity of the visual system. This may be thought of as the ability of the eye to see fine detail. Visual acuity is limited by aberrations, diffraction, and photoreceptor density in the eye. Previous studies have concluded that human optical aberrations can be influenced by the pupil size, age and the refractive surfaces of the eye.

The aberration map can be reconstructed from measures of the eye's wavefront. Typically the measures are taken using a wavefront aberrometer. The outputs of the majority of the devices are aberrations maps and several metrics, as pupil diameter and the zernike coefficients. Normally these maps and metrics are not sufficient to predict visual acuity (Figure 14.17).

In order to predict visual acuity we implemented *an algorithm that reconstructs the eye's wavefront by fitting the zernike coefficients to the zernike polynomials.*

The computational simulation was tested using both synthetic data and real data from examinations performed with a ZywaveTM wavefront aberrometer from ALM – Oftalmolaser Medical Center.

By studying optical aberrations we can estimate not only visual acuity, but also plan ways to correct it. It is also possible to compare different lenses and different surgery techniques.

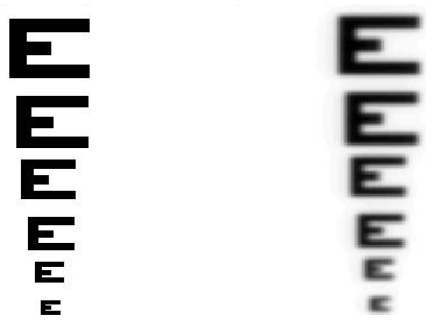

Figure 14.17 - Left: original image – Snellen Chart; Right: the same image degradated due aberration plotted in the left eye of a woman. Metric 36/6 means that the eye is able to see at 6 meters what the "standard eye" sees at 36 meters.

[6] Work performed in collaboration with António Castanheira Dinis (CECV-FML), João Nascimento (Instituto Gama Pinto), Pedro Reis (ALM).